communications earth & environment

Article

A Nature Portfolio journal

https://doi.org/10.1038/s43247-025-02825-w

Detectable ship tracks account for just 5% of aerosol indirect forcing from ship emissions

Tianle Yuan [1,2] ✉, Hua Song [1,3], Lili F. Boss[4] & Michael S. Diamond [4]

Ship emissions are a major source of aerosols over oceans, affecting both air quality and energy balance of the climate. However, estimates of their climate forcing diverge between studies relying on visible ship-tracks and those based on models. Here we show that forcing due to visible ship-tracks accounts for just 5% of the total forcing over the southeast Atlantic shipping-lane. Most forcing from ship emissions comes from aerosols that do not form detectable ship-tracks. They are only tips of the iceberg. We make three forcing calculations, one bottom-up based on visible ship-tracks, one top-down based on spatial relationships, and a hybrid approach that combines top-down or model estimated cloud droplet number concentration changes and cloud adjustments. Although the forcing based on machine learning detected ship tracks is an order of magnitude greater than prior results using manually detected ship-tracks, it remains only 5% of that inferred by top-down or cloud adjustment based methods for pre-2020 shipping. The top-down and the combined cloud adjustments methods show similar forcing for the post-2020 reduction in ships' sulfur emission, although the methods have important regional differences in cloud adjustments that need further investigation. Our results reconcile a long-standing discrepancy in the literature and have important implications for aerosol indirect forcing and marine cloud brightening.

Ship emissions are the largest source of anthropogenic SO_2 over the ocean, and they accounted for more than 10% of total anthropogenic SO_2 emissions during the 2010s[1]. Ship emissions increase the total burden of aerosol particles and thus cloud droplet number concentration (N_d) in marine clouds. Increased N_d can modify cloud properties such as cloud brightness[2], amount, and precipitation[3], which leads to changes in Earth's energy balance and creates a climate forcing. One of the clearest manifestations of these aerosol-cloud interactions is ship-tracks[4], quasi-linear features embedded in marine low clouds that often appear brighter than background, unaffected clouds because ship-emitted aerosols increase N_d. They are excellent natural experiments to study aerosol-cloud interactions[5–7].

However, it is challenging to estimate the magnitude of the total aerosol indirect forcing due to ship emissions (AIF-ship), and large uncertainty remains in its estimates. For example, Capaldo et al.[8] estimates AIF-ship to be $-0.11\ \mathrm{Wm^{-2}}$ with a global chemical transport model. Lauer et al.[9] uses a global climate model to simulate the radiative forcing of ship emissions and estimates it to be between -0.6 and $-0.19\ \mathrm{Wm^{-2}}$, depending on the emissions database used. Peters et al.[10] estimates the radiative forcing to be -0.45 to $-0.08\ \mathrm{Wm^{-2}}$ using a global model. Observational studies, however, generally show much lower estimates. An observational study aggregating manually detected ship-tracks from the "bottom-up" determines the AIF-ship to be -0.4 to $-0.6 \times 10^{-3}\mathrm{Wm^{-2}}$[11]. Peters et al.[12] also fails to detect the effect of ship emissions from the "top-down" on large-scale satellite observed cloud properties upstream and downstream of several busy shipping corridors where characteristic low-level winds blow perpendicular to the corridors.

Estimates of global AIF-ship, therefore, differ more than 1000 times (-0.6 VS $-0.4 \times 10^{-3}\mathrm{Wm^{-2}}$). The large discrepancy has important implications for estimates of total AIF and climate engineering techniques such as marine cloud brightening (MCB)[13–15]. One important question is whether and how results from ship-tracks can be scaled up to estimate global AIF and AIF-ship. Moreover, ship-tracks are widely considered as analogues for MCB (ref. 16). Were AIF-ship much weaker than what is estimated in modeling results and instead agreed with what observational studies have shown, it would suggest MCB may not be viable given the small impact from large ship emissions. It is imperative to improve our understanding of this large discrepancy, which can help reduce the uncertainty of AIF in general and benefit MCB studies.

[1]Earth Science Division, NASA Goddard Space Flight Center, Greenbelt, MD, USA. [2]GESTAR-II, University of Maryland, Baltimore County, Baltimore, MD, USA. [3]SSAI Inc., Lanham, MD, USA. [4]Department of Earth, Ocean, and Atmospheric Science, Florida State University, Tallahassee, FL, USA. ✉e-mail: tianle.yuan@nasa.gov

Recent advances offer tools to do so. Automated ship-track detection using deep learning techniques detects more samples than those using manual methods[11,17] by orders of magnitude[18,19]. Global model results could bias towards higher AIF-ship values because they often simulate stronger increases of cloud liquid water path in response to added aerosols than observations (e.g.,[15,17,20,21]), which may help explain part of the discrepancy.

At the same time, top-down statistical analyses of climatological satellite retrievals provide novel observational estimates on the AIF-ship for the southeast Atlantic (SEA) region[22], where low-level winds blow parallel to a major shipping corridor and keep pollution relatively spatially constrained, with results suggesting a strong regional forcing in line with that produced by climate models[9].

Shipping fuel regulations from the International Maritime Organization that took effect in 2020 (IMO2020) have already resulted in a decrease in ship-track formation[18] and detectable microphysical signatures in the SEA shipping corridor[23]. Combining estimated N_d changes from a chemical transport and machine learning models with meteorology-dependent cloud fraction and liquid water path adjustments from ship-tracks[21], Yuan et al.[15] estimate the AIF-ship due to IMO2020 to be $+0.2\ \mathrm{Wm}^{-2}$, which is in better agreement with studies that use global models[8,9]. This new progress provides the opportunity to understand the disparity in previous estimates of AIF-ship. An accurate estimation of AIF-ship could also contribute to reducing the significant uncertainty surrounding total AIF[24].

Here we combine recent advances in both bottom-up and top-down approaches to study the magnitude of AIF-ship in the SEA region. The goal is to elucidate the sources of discrepancy in the literature and provide approaches that could scale up insights from small-scale experiments. Section "Closure between bottom-up and top-down estimates" presents the data and method used. Section "Decomposition of forcing components" shows our results. Discussions and conclusions are presented in Section "Discussion and conclusions".

Closure between bottom-up and top-down estimates

Method

More detailed description of our methods and data can be found in the Method and Data section. Here we briefly outline them. We derive N_d perturbations introduced by ship-emissions by multiplying the frequency of ship-track density and mean ΔN_d in a ship-track in a bottom-up (BU) estimate. ΔN_d from the top-down (TD) method is derived from geospatial krigging while it is modled in a chemical transport model by differentiating runs with and without ship emissions. AIF-Ship in BU is estimated by combining cloud adjustments with estimated ΔN_d's while in a TD method, it is also estimated by krigging. BU methods are differentiated by their sources of ΔN_d that include TD, ship-track density, and modeled. We examine the closure of AIF-ship between BU and TD methods.

Results

Figure 1A shows the MODIS derived N_d map for the southeast Atlantic region during the September, October and November (SON) season when the impact of ship emission is most prominent[22]. The counterfactual N_d climatology map from TD (see Methods) without the influence of ship emissions is shown in Fig. 1B, and the difference between the observed and counterfactual values, interpreted as the causal effect of shipping, is shown in Fig. 1C. The core shipping lane, following the definition in Diamond et al.[23], is highlighted as the area covered by white dots. The southern tip of this core lane, south of 15S, is less well defined in terms of N_d, possibly because the control N_d is even higher to the east of the core lane.

Figure 1D shows the frequency of visible ship-track pixels as a percentage of all MODIS observations, f_{ST}. The peak frequency is around 2% for this region, more than 20 times higher than what is reported in ref. 11. f_{ST} shows a well-defined shipping lane and its distribution aligns well with the core shipping lane in Fig. 1A. These two distributions are independently derived.

Comparing the distributions of N_{clim} (Fig. 1A) and f_{ST}, we note that f_{ST} becomes near zero at around 9°S while the elevated N_{clim} values reaches further north at around 5°S, possibly due to unfavorable cloud types for detection at these tropical regions[18].

Figure 1E shows ΔN_d using BU-ST, which also features a well-defined shipping lane shape and aligns well with the Diamond et al.[23] definition, albeit showing a broader lane. Its centerline shifts around 1° to the downwind (west) side at several latitudes. ΔN_d from BU-ST peaks at 0.5–1 cm^{-3}, an order of magnitude smaller than the TD ΔN_d whose peak is around 10 cm^{-3}. BU-ST likely underestimates the ΔN_d because ship-emitted aerosols do not always form detectable ship-tracks. In addition, the "background" used (see Methods) is a mixture of actual background values and clouds affected by ship emissions that do not form visible ship-tracks. Both factors make the BU-ST density likely to severely underestimate ΔN_d.

Next we compare estimates of AIF-ship in the SEA during SON season using the manually-logged tracks of Schreier et al.[11], our BU-ST method

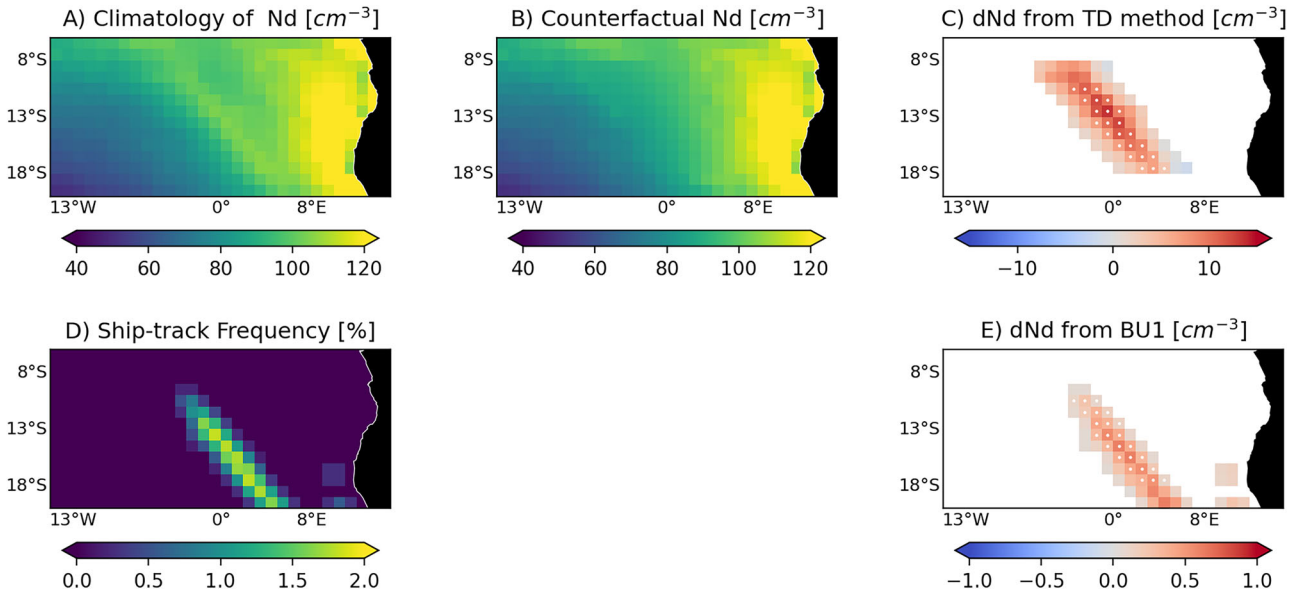

Fig. 1 | ΔNd estimated using BU and TD methods. Spatial maps of **A** climatology of N_d with the shipping lane visible as a line of elevated N_d; **B** Counterfactual N_d from TD without the impact of ship emissions; **C** ΔN_d from TD, i.e., N_d from A minus N_d from B; **D** ship-track frequency as a percentage of total observations; **E** ΔN_d derived by multiplying ship-track frequency and N_d perturbation from each ship-track (BU-ST N_d).

(with ML-detected tracks), and our TD method as well as a hybrid approach taking the ΔN_d values from TD and cloud adjustments from the ML-detected ship-tracks[21]. For the hybrid BU-TD approach, we use two functional forms of LWP and Cf adjustments: Adj;= $f(N_d$, Cf) or Adj = $f(N_d)$, because Cf adjustment is more sensitive to the choice of these parameters and the two forms usually represent the upper and lower bounds[15,21].

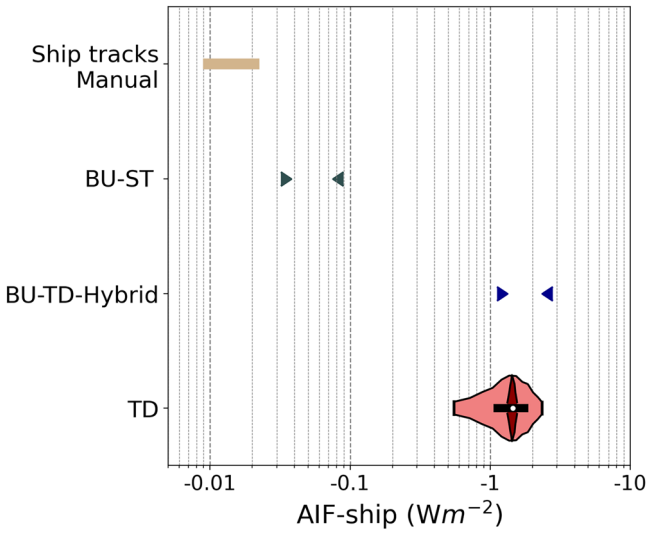

Fig. 2 | Climatological AIF-ship estimates from BU-ST, BU-TD-Hybrid, and TD during the SON season, as well as one year of ship-track detections using manual labels from ref. 11. The x-axis uses log-scale. Uncertainty for the BU methods is represented by the spread in the triangle markers, each representing a different set of background meteorology variables used to calculate the adjustments. Uncertainty for the TD method is quantified as the 95% confidence interval of simulated counterfactual fields for the Twomey effect only (dark red violin plot) and for AIF-ship including adjustments (light red violin); the black line and white circle represent the interquartile range and mean, respectively.

The results are shown in Fig. 2. Our BU-ST estimate is about an order of magnitude larger than the previous estimate from Schreier et al.[11], but more than an order of magnitude smaller than that from TD (and thus also BU-TD), regardless of which adjustment functional form we choose. The order of magnitude difference between BU-ST and TD is in line with the estimated ΔN_d difference between BU-ST and TD in Fig. 1. The order of magnitude difference between BU-ST and previous BU estimate is also consistent with the f_{ST} difference between BU-ST and[11]. TD and BU-TD estimate AIF-ship to be around –2 Wm^{-2} in the SEA during SON, with much of the uncertainty coming from cloud adjustments. Our results show that visible ship-tracks only represent ~5% the total indirect forcing from ship emissions. They represent only tips of the iceberg.

Decomposition of forcing components

In Fig. 3, we show maps of total AIF-ship and its components, i.e., the Twomey effect, the LWP adjustment, and the cloud fraction adjustment, using the BU-ST, BU-TD hybrid, and TD methods. BU-ST again estimates the lowest AIF-ship because of the ΔN_d underestimation since not all emissions lead to detectable ship-tracks. Mean AIF-ship averaged over the shipping lane from BU-TD and TD are closer to each other at approximately −2.5 Wm^{-2} and −1.5 Wm^{-2}, respectively, over the core corridor (C) but there are clear differences in their breakdowns and spatial distributions. The BU and hybrid results show uniformly positive cloud fraction adjustments (negative forcing) and negative liquid water path adjustments (positive forcing), whereas the TD results show a clear and strong north-south contrast featuring positive cloud fraction adjustments in the north (N) and negative LWP adjustments in the south (S). The net result is much stronger cooling in the northern region (10°–14°S) and much weaker cooling in the southern region (14°–18°) than that of BU-TD.

In Fig. 4, we show estimates of forcing due to the IMO2020, i.e., AIF-IMO2020 during the SON season. For BU-ST, we calculate ΔN_d due to IMO2020 by first calculating changes in f_{ST} between the climatological mean and 2020 and then multiplying it with ΔN_d using equation 3 (see *Method*). For the hybrid BU-GEOS method, we use the modeled IMO2020-induced ΔN_d from Yuan et al.[15]. In 2020, detectable ship-tracks strongly decreased in

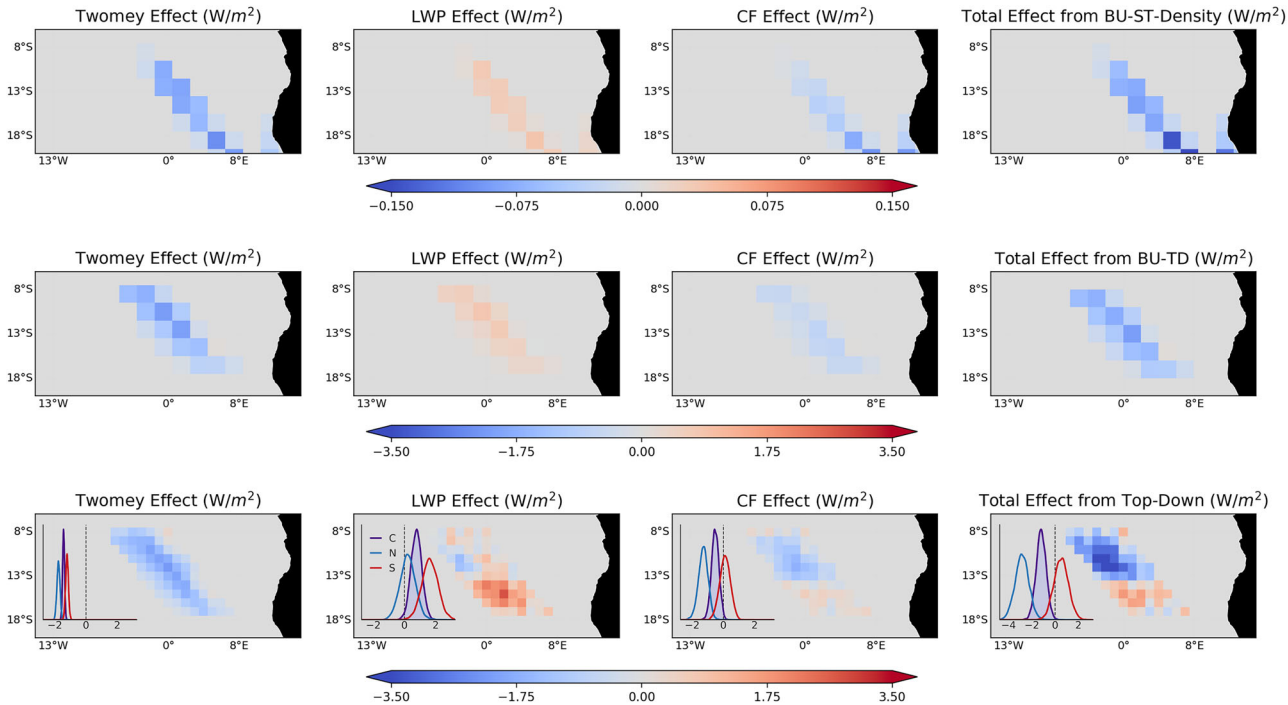

Fig. 3 | Estimated AIF-ship maps. BU-ST is shown in the top row, BU-TD in the middle row, and TD in the bottom row. The Twomey effect, liquid water path and cloud fraction adjustments, and their net effective forcing are shown as the columns from left to right. Insets in the bottom row show the TD results broken down by averaging over the core corridor (C), 10°–14° S (N), or 14°–18° (S) (see Fig. S2 for more details).

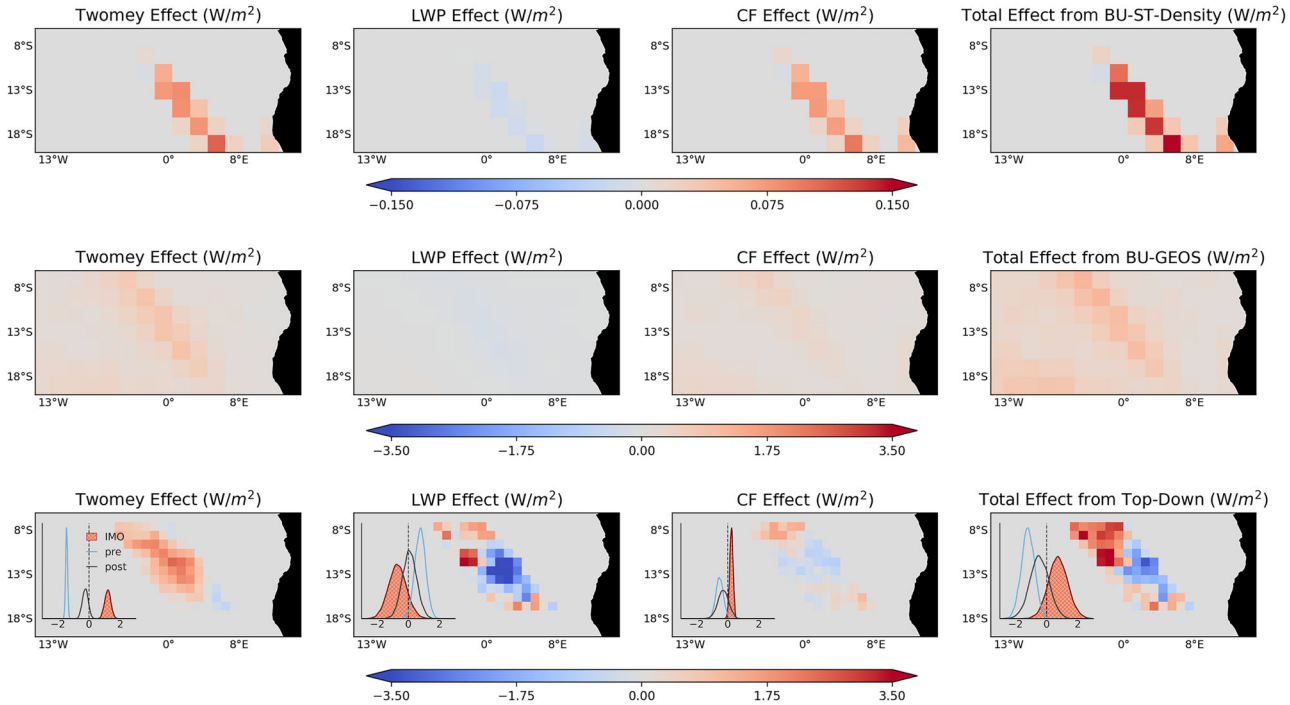

Fig. 4 | As in Fig. 3, but for the estimated AIF-ship map due to IMO2020 regulations. Insets in the bottom row here represent core corridor values from the pre- and post-2020 periods and their difference (IMO effect; see Fig. s3 for more details on the inset.).

this region Yuan et al.[21]. Yet, BU-ST estimates total AIF-IMO2020 to be around $+0.11\ \mathrm{Wm}^{-2}$ within the shipping lane. That is again almost an order of magnitude smaller than the BU-GEOS and TD estimates of just under $+1\ \mathrm{Wm}^{-2}$. TD again displays a seemingly dipole pattern in the AIF-IMO2020, albeit with a substantial degree of noise from the limited temporal sampling[22]. BU-GEOS also has a slight and gradual north-south change in both the LWP and the Cf adjustments, but its magnitude is much more muted compared to the contrast in TD. Whereas the TD magnitude is dominated by the Twomey effect due to near-perfect cancellation between the liquid water path and cloud fraction adjustments, in BU-GEOS, the cloud fraction adjustment contributes substantially to the effective forcing. It is worth noting that in the broader SEA region, there are multiple shipping lanes and BU-GEOS estimates significant AIF-IMO2020 from them other than the one discussed in above figures. Their contributions put the overall AIF-IMO2020 in the broader SEA region stronger than only considering the central shipping lane Yuan et al.[15].

The decomposition and its spatial distributions still have important differences between BU and TD methods that need to be resolved.

Discussion and conclusions

Our results show that the forcing estimate based on explicitly detectable ship-tracks represent less than 5% of the total AIF-ship based on either top-down or hybrid methods with top-down or model-based microphysics and bottom-up macrophysical cloud adjustment estimates. Our closure study thus reveals that visible ship-tracks represent only the tips of the iceberg that is the total aerosol effective radiative forcing through ACI. Several factors can prevent ship emissions from forming detectable ship-tracks such as unfavorable cloud conditions[18], weak emission rates that do not affect clouds enough to be visible, or background clouds that are already not aerosol-limited[18,25]. Heterogeneous background cloud fields, especially in deeper boundary layers, provide a particular challenge for detecting aerosol perturbations without prior knowledge of where the plume has spread[26] and once-compact plumes spread into the "background" over time[27].

Instead, it appears that ship emissions realize their forcing primarily through increasing N_d in terms of diffused and undetected plumes. Given the level of agreement between the TD and BU-GEOS methods regarding AIF-IMO2020, both the global AIF-Ship and its reduction post-2020 should be on the order of $-0.1\ \mathrm{Wm}^{-2}$, which agrees with global model estimates. This is also crucial for designing the deployment and assessing the impact of MCB; detecting and attributing the impact of an MCB experiment will need to consider the total effect instead of visible tracks. Virtual ship-tracks have been used to address the impact of undetected ship-tracks[25]. However, this approach has important assumptions and errors that affect the derived cloud adjustments[28,29].

The consistent forcing estimates of AIF-IMO2020 from BU-GEOS and TD are encouraging because they are completely independent. The BU-GEOS and TD approaches thus also provide an independent check and validation for each other. Both approaches provide valuable estimates of AIF and the potential efficacy of MCB, at least in stratocumulus clouds.

It is also important to investigate and resolve the clear differences in geographic distributions of cloud adjustments between the two methods. In particular, LWP and Cf adjustments show major disagreements between the two approaches in terms of their geographic distribution and the very large uncertainties on the TD results complicate their physical interpretation. Several factors could contribute to this difference such as uncertainties in cloud retrievals, uncertainties and assumptions in the TD geospatial kriging algorithm, and uncertainty of scaling cloud adjustments at ship-track scale to larger scales. Cloud retrievals in this area can also be strongly affected by the presence of absorbing aerosols above low level clouds[30], which could affect the pattern of cloud adjustment estimates from kriging if there is a systematic difference in above-cloud absorbing optical depth between the north and south of the domain. We leave further investigations into such factors to follow-up studies.

The BU and TD approaches analyzed here thus have complementary strengths and weaknesses. The overall strength of the ΔN_d perturbation is not recoverable from the BU approach alone while the TD values and modeling results are based on observations and modeling of processes. However, the TD adjustment values are very poorly constrained compared to the relationships derived BU from visible ship-tracks. A combined TD-BU approach may thus offer the best path for quantifying AIF-ship in this region, if it can be shown that the adjustment relationships derived using visible ship-tracks generalize to undetected perturbations. Indeed, if it can be shown that cloud

adjustments and their dependence on background cloud and environmental conditions based on large number of ship-tracks under diverse conditions[21] offer good approximation of cloud adjustments at larger scales, hybrid methods combining cloud microphysical estimates with parameterized adjustments could prove useful not just for the IMO2020 problem[15], but also historical aerosol indirect forcing more broadly.

To summarize, we conduct a closure study that compares bottom-up approaches with a top-down approach in estimating AIF-ship in the SEA. We show that visible ship-tracks represent only a small fraction, around 5%, of the total forcing. On the other hand, analyses of visible ship-tracks are valuable because they provide functions of cloud LWP and Cf adjustments to N_d. Our results resolve the outstanding large disparity in the literature between observation-based and modeling estimates of AIF-ship in the SE Atlantic, which should apply over other regions. The strong underestimate by previous studies is mostly due to two factors. First, detection of ship tracks is an order of magnitude lower than the current state of the art; second, the assumption that visible ship-tracks represent the majority of the impact is incorrect. Most of the forcing appears to come from diffusion of aerosols that do not form readily detectable ship-tracks.

Method and data

Bottom up methods

We study the impact of emissions in the SEA shipping lane using two sets of opportunities and estimate AIF-ship. The two opportunities are changes induced by IMO2020 and the long-term climatology. We compare estimates of AIF-ship from bottom-up approaches, a top-down approach, and hybrid approaches that combines bottom-up cloud adjustments with microphysical perturbations from the top-down method or a chemistry-climate model, to better constrain AIF-ship and understand the discrepancy in the literature. The top-down approach uses geospatial krigging to create counterfactual distributions of cloud properties with and without the influence of ship emissions (refs. 22,23), referred to as the TD method in the following. The difference between the observed and the counterfactual is taken as the impact of ship emissions on clouds.

In both the bottom-up and hybrid approaches, we combine cloud adjustments in liquid water path (LWP) and cloud fraction (Cf) derived from Yuan et al.[21] with estimated perturbations in N_d, i.e., ΔN_d, to estimate AIF-ship (refs. 15,17,21. Briefly, the scene albedo sensitivity to N_d can be determined by:

$$\begin{aligned} S^* &= \frac{dA}{dN_d} = \frac{d\left(A_{ac}Cf_{total} + A_s\left(1 - Cf_{total}\right)\right)}{dN_d} \\ &\approx Cf \times S + \left(1 - Cf_{high}\right) \times \frac{dCf}{dN_d} \times \left(A_{ac} - A_s\right) \end{aligned} \quad (1)$$

where A, A_{ac}, Cf_{totab} A_s, Cf, and Cf_{high} are the scene albedo, cloud albedo, total cloud fraction, surface albedo, low cloud fraction, and high cloud fraction, respectively. S is cloud albedo sensitivity to N_d:

$$S = \frac{dA_c}{dN_d} = \frac{A_c(1 - A_c)}{3N_d} \times \left(1 + \frac{5}{2}\frac{dln\,LWP}{dln\,N_d}\right). \quad (2)$$

$\frac{dln\,LWP}{dln\,N_d}$ and $\frac{dCf}{dN_d}$ are derived from ship-track analysis Yuan et al.[21]. Together with observations of clouds, surface, and ΔN_d, we can calculate AIF-ship. For more details, please refer to these two refs. 15,21.

The bottom-up and hybrid approaches differ in the sources of ΔN_d. In the BU-ST, we use the frequency of visible ship-tracks and cloud properties of background and ship-track pixels to calculate ΔN_d due to ship emissions. The derived ΔN_d is then used to calculate the AIF-ship in the shipping lane. ΔN_d can be estimated as

$$\Delta N_d = f_{ST}(\overline{N_{ST}} - \overline{N_{BG}}), \quad (3)$$

where $\overline{N_{ST}}$ and $\overline{N_{BG}}$ are average N_d's for ST and background pixels, respectively, and f_{ST} is fraction of pixels that are visible ship-tracks. Following a similar procedure, we can derive the difference between shipping lane and background in other variables. This BU-ST approach assumes the AIF-ship mostly comes from visible ship-tracks.

In the BU hybrid approach, we couple cloud adjustments to N_d perturbations from alternative sources including ΔN_d from TD, dubbed BU-TD, and ΔN_d simulated by NASA's Global Earth Observing System (GEOS) with the Goddard Chemistry Aerosol Radiation and Transport (GOCART) aerosol module, using two separate neural-network models to convert modeled aerosol optical depth to cloud condensation nuclei (CCN) and CCN to N_d for IMO2020[15], dubbed BU-GEOS. In the case of the climatology, we use the same ΔN_d derived from TD to calculate AIF-ship. It assumes that the cloud adjustments derived from ship-tracks can be applied to large-scale AIF calculations and that AIF-ship results from all impacts of ship emissions on N_d, including both those that form ship-tracks and those that do not[7,18].

The uncertainty and assumptions of the BU methods can be found in previous studies Toll et al.[17], Yuan et al.[15], Yuan et al.[21]. To quantify uncertainty in this study, we calculate the LWP and Cf adjustments separately for a case based on binning the ship tracks by background N_d only and a case using 2D binning by background N_d and Cf. These binning choices produced the largest spread in estimates in previous work Yuan et al.[15], Yuan et al.[21].

Top-down method

The top-down method of universal kriging for the southeast Atlantic shipping corridor was introduced in Diamond et al.[22] and refined in Diamond et al.[23]. Kriging is a classic geostatistical method[31] in which values at unknown locations are estimated based on the spatial relationship between known values of a given variable. In universal kriging, a mean function is fit on the spatial location (here, latitude, longitude, their squares, and their product) and other co-variates (here, the cloud controlling factors of sea surface temperature, estimated inversion strength, and surface wind speed) and then errors are assumed to be spatially correlated based only on their distance from nearby values, as quantified via an empirical semivariogram. Grid boxes surrounding the SEA shipping corridor are treated as unknown and their neighbors, assumed to be unaffected by shipping, are used to fit the kriging algorithm that predicts a counterfactual field of what values would have looked like in the absence of shipping. Uncertainty is quantified via simulation of 5000 counterfactual kriged fields consistent with the fitted parameters. Because the creation of the counterfactual relies on interpolation from the background and errors are related to spatial variability of the background, relatively smooth background fields are needed for the counterfactual to be well constrained. Constraints are generally weak when only a few years of data are available. For further details and the uncertainties of the method, readers are referred to Diamond et al.[22] and Diamond et al.[23].

Data

We use cloud retrievals from the MODerate resolution Imaging Spectrometer (MODIS) instrument on board Aqua that include droplet effective radius (R_{eff}), cloud optical depth (τ), Cf_{total}, Cf, and Cf_{high}, We derive N_d and LWP using R_{eff} and τ[32,33]. Both Level2 instantaneous and L3 month mean data are used here. Radiative fluxes, solar incoming fluxes, and cloud and surface albedo from the Clouds and the Earth's Radiant Energy System (CERES) Energy Balanced and Filled (EBAF) version 4.1 are obtained to calculate AIF-ship[34]. Cloud fraction for the TD method is from the CERES/Aqua Single-Scanner Footprint monthly regional product[34]. visible ship-tracks from Aqua MODIS is used to calculate f_{ST} and cloud properties of polluted cloud pixels and background clouds[19,21].

In BU-ST, we use visible ship-track masks and corresponding MODIS pixel level N_d to obtain ΔN_d for the period between 2003 and 2019 with equation 3. ΔN_d introduced by IMO2020 is taken as the difference in simulated N_d by a global chemical transport model between with and without IMO2020 fuel regulation's impact on emissions[15]. Together they are used to calculate forcing using the cloud adjustment approach.

Data availability

The MODIS cloud product, CERES flux and albedo product, and the MERRA2 data used in this study are available from the Atmosphere Archive and Distribution System (LAADS) Distributed Active Archive Center (DAAC) (https://ladsweb.nascom.nasa.gov/), CERES, and the Global Modeling and Assimilation Office (https://gmao.gsfc.nasa.gov/reanalysis/MERRA-2/data_access/). Ship-track block data used in this analysis is staged at https://doi.org/10.7910/DVN/JII4DN.

Received: 23 June 2025; Accepted: 23 September 2025;
Published online: 14 November 2025

References

1. Hoesly, R. M. et al. Historical (1750–2014) anthropogenic emissions of reactive gases and aerosols from the Community Emissions Data System (CEDS). *Geosci. Model Dev.* **11**, 369–408 (2018).
2. TWOMEY, S. Pollution and the planetary albedo. Atmospheric Environment (1967) (1974). http://www.sciencedirect.com/science/article/pii/0004698174900043.
3. Albrecht, B. Aerosols, cloud microphysics, and fractional cloudiness. *Science* **245**, 1227 (1989).
4. Conover, J. H. Anomalous cloud lines. *J. Atmos. Sci.* **23**, 778–785 (1966).
5. Coakley, J. A., Bernstein, R. L. & Durkee, P. A. Effect of ship-stack effluents on cloud reflectivity. *Science* **237**, 1020–1022 (1987).
6. Hobbs, P. V. et al. Emissions from ships with respect to their effects on clouds. *J. Atmos. Sci.* **57**, 2570–2590 (2000).
7. Christensen, M. W. et al. Opportunistic experiments to constrain aerosol effective radiative forcing. *Atmos. Chem. Phys.* **22**, 641–674 (2022).
8. Capaldo, K., Corbett, J. J., Kasibhatla, P., Fischbeck, P. & Pandis, S. N. Effects of ship emissions on sulphur cycling and radiative climate forcing over the ocean. *Nature* **400**, 743–746 (1999).
9. Lauer, A., Eyring, V., Hendricks, J., Jöckel, P. & Lohmann, U. Global model simulations of the impact of ocean-going ships on aerosols, clouds, and the radiation budget. *Atmos. Chem. Phys.* **7**, 5061–5079 (2007).
10. Peters, K., Stier, P., Quaas, J. & Graßl, H. Aerosol indirect effects from shipping emissions: sensitivity studies with the global aerosol-climate model ECHAM-HAM. *Atmos. Chem. Phys.* **12**, 5985–6007 (2012).
11. Schreier, M., Mannstein, H., Eyring, V. & Bovensmann, H. Global ship track distribution and radiative forcing from 1 year of AATSR data. *Geophys. Res. Lett.* **34**, https://agupubs.onlinelibrary.wiley.com/doi/abs/10.1029/2007GL030664 (2007).
12. Peters, K., Quaas, J. & Graßl, H. A search for large-scale effects of ship emissions on clouds and radiation in satellite data. *J. Geophys. Res. Atmos.* **116**, https://agupubs.onlinelibrary.wiley.com/doi/abs/10.1029/2011JD016531 (2011).
13. Latham, J. et al. Marine cloud brightening. *Philos. Transac. R. Soc. A: Math. Phys. Eng. Sci.* **370**, 4217–4262 (2012).
14. Diamond, M. S. et al. To assess marine cloud brightening's technical feasibility, we need to know what to study-and when to stop. *Proc. Nat. Acad. Sci. USA* **119**, e2118379119 (2022).
15. Yuan, T. et al. Abrupt reduction in shipping emission as an inadvertent geoengineering termination shock produces substantial radiative warming. *Commun. Earth Environ.* **5**, 1–8 (2024).
16. Robock, A., MacMartin, D. G., Duren, R. & Christensen, M. W. Studying geoengineering with natural and anthropogenic analogs. *Clim. Change*, http://link.springer.com/article/10.1007/s10584-013-0777-5 (2013).
17. Toll, V., Christensen, M., Quaas, J. & Bellouin, N. Weak average liquid-cloud-water response to anthropogenic aerosols. *Nature* **572**, 51–55 (2019).
18. Yuan, T. et al. Global reduction in ship-tracks from sulfur regulations for shipping fuel. *Sci. Adv.* **8**, eabn7988 (2022).
19. Yuan, T. et al. Automatically finding ship tracks to enable large-scale analysis of aerosol-cloud interactions. *Geophys. Res. Lett.* **46**, 7726–7733 (2019).
20. Malavelle, F. F. et al. Strong constraints on aerosol–cloud interactions from volcanic eruptions. *Nature* **546**, 485–491 (2017).
21. Yuan, T. et al. Observational evidence of strong forcing from aerosol effect on low cloud coverage. *Science Advances* **9**, eadh7716 (2023).
22. Diamond, M. S., Director, H. M., Eastman, R., Possner, A. & Wood, R. Substantial Cloud Brightening From Shipping in Subtropical Low Clouds. *AGU Adv.* **1**, e2019AV000111 (2020).
23. Diamond, M. S. Detection of large-scale cloud microphysical changes within a major shipping corridor after implementation of the International Maritime Organization 2020 fuel sulfur regulations. *Atmos. Chem. Phys.* **23**, 8259–8269 (2023).
24. Forster, P. et al. The Earth's Energy Budget, Climate Feedbacks, and Climate Sensitivity. In *Climate Change 2021: The Physical Science Basis. Contribution of Working Group I to the Sixth Assessment Report of the Intergovernmental Panel on Climate Change* (Cambridge University Press, 2021).
25. Manshausen, P., Watson-Parris, D., Christensen, M. W., Jalkanen, J.-P. & Stier, P. Invisible ship tracks show large cloud sensitivity to aerosol. *Nature* **610**, 101–106 (2022).
26. Possner, A., Wang, H., Wood, R., Caldeira, K. & Ackerman, T. P. The efficacy of aerosol–cloud radiative perturbations from near-surface emissions in deep open-cell stratocumuli. *Atmos. Chem. Phys.* **18**, 17475–17488 (2018).
27. Goren, T. & Rosenfeld, D. Satellite observations of ship emission induced transitions from broken to closed cell marine stratocumulus over large areas. *J. Geophys. Res. Atmos.* **117**, D17206 (2012).
28. Tippett, A., Gryspeerdt, E., Manshausen, P., Stier, P. & Smith, T. W. P. Weak liquid water path response in ship tracks. *Atmos. Chem. Phys.* **24**, 13269–13283 (2024).
29. Yuan, T. et al. Analyses of virtual ship-tracks systematically underestimate aerosol-cloud interactions signals. *Geophys. Res. Lett.* **52**, e2024GL114356 (2025).
30. Meyer, K., Platnick, S. & Zhang, Z. Simultaneously inferring above-cloud absorbing aerosol optical thickness and underlying liquid phase cloud optical and microphysical properties using MODIS. *J. Geophys. Res. Atmos.* **120**, 5524–5547 (2015).
31. Zimmerman, D., Stein, M., Gelfand, A. & Diggle, P. Classical geostatistical methods. *Handbook Spatial Stat.* 29–44 (2010). https://doi.org/10.1201/9781420072884.
32. Platnick, S. et al. The MODIS cloud optical and microphysical products: collection 6 updates and examples from terra and aqua. *IEEE Trans. Geosci. Remote Sens.* **55**, 502–525 (2017).
33. Grosvenor, D. P. et al. Remote sensing of droplet number concentration in warm clouds: a review of the current state of knowledge and perspectives. *Rev. Geophys.* **56**, 409–453 (2018).
34. Loeb, N. G. et al. Clouds and the Earth's Radiant Energy System (CERES) Energy Balanced and Filled (EBAF) Top-of-Atmosphere (TOA) Edition-4.0 Data Product. *J. Clim.* **31**, 895–918 (2018).

Acknowledgements

TY, HS, and MSD acknowledge funding from the NOAA Climate Program Office (CPO) Earth's Radiation Budget (ERB), Atmospheric Chemistry, Carbon Cycle, and Climate (AC4), and Climate Variability and Predictability (CVP) Programs, Grants NA23OAR4310298, NA23OAR4310299, and NA23OAR4310297, respectively. TY additionally acknowledges funding support from NASA (grant numbers 80NSSC24K0458 and 80NSSC24M0045) and DOE (grant DE-SC0024078).

Author contributions

TY and MSD conceived the idea and developed the methodology. TY led the bottom-up analysis and wrote the original manuscript. LFB and MSD led the top-down analysis. HS curated and processed satellite data and created the

figures. HS, LFB, and MSD contributed to the review and editing of the manuscript.

Competing interests
The authors declare no competing interests.

Additional information
Supplementary information The online version contains supplementary material available at https://doi.org/10.1038/s43247-025-02825-w.

Correspondence and requests for materials should be addressed to Tianle Yuan.

Peer review information *Communications Earth and Environment* thanks the anonymous reviewers for their contribution to the peer review of this work. Primary Handling Editors: Zijun Li and Alice Drinkwater. [A peer review file is available].